New experimental data on excitation functions of ^{3}He-induced nuclear reactions on Ta up to 27 MeV

B. M. Ali,[1,*] Gehan Y. Mohamed,[1] F. Ditrói,[2] S. Takács,[2] and M. Al-Abyad[1]

[1]*Cyclotron Facility, Experimental Nuclear Physics Department, Nuclear Research Centre, Egyptian Atomic Energy Authority, Cairo 13759, Egypt*

[2]*Institute for Nuclear Research (ATOMKI), Debrecen H4026, Hungary*

(Received 6 May 2020; revised 24 July 2020; accepted 27 October 2020; published 9 December 2020)

Excitation functions of ^{3}He-induced nuclear reactions on ^{nat}Ta were measured utilizing the MGC-20E cyclotron, stacked-foils activation technique, and high-resolution gamma-ray spectrometry. From their threshold energies up to 27 MeV, cross sections for ^{nat}Ta(^{3}He, xn) ^{182}Re^{m}, ^{182}Re^{g}, ^{181}Re, and ^{nat}Ta(^{3}He, αxn) ^{178}Ta^{A}, ^{180}Ta^{g} reactions were measured. The half-life of the radionuclide ^{181}Re was checked experimentally. The intensity of the energy line 360.7 keV, in the radionuclide ^{181}Re decay scheme, was revised experimentally. The new experimental intensity represents about half the reported value in the different nuclear structure databases. The nuclear reaction codes TALYS-1.9 and EMPIRE-3.2.3 were used to predict the formation of these products. The isomeric cross-section ratio for the ^{182}Re^{m,g} was also calculated. The ratio indicates that the pre-equilibrium mechanism is dominant at energies over 19 MeV. Various combinations of the models' parameters implemented in EMPIRE such as nuclear level density models, optical model, and pre-equilibrium parameters were used to reproduce the experimental excitation functions. For TALYS calculations, the TENDL-2019 nuclear data library based on TALYS-1.9 was used. The present data were compared to theoretical results and the available experimental data. Integral yields for the produced radioisotopes were determined.

DOI: 10.1103/PhysRevC.102.064608

I. INTRODUCTION

Studies of excitation functions of nuclear reactions are of considerable importance for constructing experimental nuclear reaction databases and testing/verifying evaluated nuclear reaction data from different nuclear reaction models. They are also useful, from a radionuclide production point of view, in optimizing production for practical and medical applications [1]. Lastly, they could also be considered as an effective means for testing and correcting nuclear structure and decay databases; see, e.g., [2]. This work is part of a systematic study of excitation functions of ^{3}He-particle-induced nuclear reactions on different materials intended to build a ^{3}He activation library for the different applications. Nuclear reactions induced by ^{3}He particles suffer a lack of experimental data due to many reasons, the most important of which is the high cost of ^{3}He gas. This lack of experimental data limits the reliability of data evaluation so that it cannot be used securely for sensitive applications.

Tantalum is a very important transition metal considered due to its high melting point and hardness, as one of the refractory metals group [3]. It has a lot of applications in different fields and is regarded as a technology-critical element [4]. Natural tantalum consists mainly from ^{181}Ta with 99.988% abundance. The rest with 0.012% abundance consists of the very long-lived isomeric state ^{180}Ta^{m} ($T_{1/2} = 7.15 \times 10^{15}$ y) [5]. Therefore, natural tantalum targets could be considered to a high extent as enriched ^{181}Ta targets and then cross sections of induced nuclear reactions on natural tantalum targets represent isotopic cross sections. A significant amount of data were found in the literature for proton, deuteron, and alpha activation of tantalum. For ^{3}He-induced nuclear reactions only three experimental works were found [6–8]. Scott *et al.* [6] irradiated natural tantalum by 33 MeV ^{3}He particles to study the (^{3}He, xn), (^{3}He, α), and (^{3}He, $2n\alpha$) nuclear reactions, $x = 1$–4. Their study was about the comparison between mechanisms of nuclear reactions induced by ^{3}He and ^{4}He particles on heavy target nuclei. Although they declared that they resolved the activities of the isomeric pair ^{182}Re^{m,g}, they only presented one cross-section data set for ^{182}Re production. Hermes *et al.* [7] studied the mechanisms of (^{3}He, xn), $x = 3$–7, induced reactions by 75-MeV ^{3}He particles on ^{181}Ta and ^{197}Au. They performed two separate irradiations; one with 26.4-MeV ^{3}He particles from Van de Graff on single target foil and the other utilizing the stacked-foils technique with 75-MeV ^{3}He particles at the external beam of a synchrocyclotron. Nagame *et al.* [8] irradiated tantalum targets by 65-MeV ^{3}He particles. They presented the excitation function of the nuclear reaction ^{181}Ta(^{3}He, n) while studying the reaction mechanisms of the (^{3}He, n) channel using a variety of targets. Although these studies collectively covered ^{3}He-induced nuclear reactions on tantalum for a large energy range, they were performed 30–50 years ago. As a result, both the half-lives of the resulting radionuclides and the intensity of the emitted gamma rays have changed significantly in the intervening years. In the present work, the nuclear reactions ^{181}Ta(^{3}He, x) ^{182}Re^{m,g}, ^{181}Re, ^{178}Ta^{A}, ^{180}Ta^{g} were identified from their respective threshold energies up to 27 MeV. The isomeric cross-section ratio (ICSR) of

*b.moh.ali@sci.asu.edu.eg

TABLE I. Target foils order in each stack in addition to the measured thickness the mean energy of each foil, and their uncertainties.

	Stack 1			Stack 2		
Foil number	Target ID	Mean-energy MeV	Areal density mg/cm^2	Target position	Mean-energy MeV	Areal density mg/cm^2
1	Ta	26.41 ± 0.39	13.62 ± 0.11	Ti	26.65 ± 0.29	5.51 ± 0.09
2	Ti	25.46 ± 0.34	5.61 ± 0.09	Ta	25.69 ± 0.43	14.54 ± 0.10
3	Ta	24.48 ± 0.50	14.17 ± 0.09	Ti	24.72 ± 0.37	5.29 ± 0.07
4	Ti	23.47 ± 0.43	5.54 ± 0.06	Ta	23.72 ± 0.55	14.01 ± 0.07
5	Ta	22.43 ± 0.62	13.74 ± 0.15	Ti	22.69 ± 0.47	5.63 ± 0.06
6	Ti	21.36 ± 0.53	5.38 ± 0.09	Ta	21.62 ± 0.67	14.78 ± 0.07
7	Ta	20.25 ± 0.75	14.02 ± 0.20	Ti	20.52 ± 0.56	5.40 ± 0.09
8	Ti	19.10 ± 0.63	4.88 ± 0.11	Ta	19.38 ± 0.80	14.25 ± 0.12
9	Ta	17.89 ± 0.89	14.84 ± 0.10	Ti	18.19 ± 0.67	5.21 ± 0.05
10	Ti	16.63 ± 0.74	5.33 ± 0.02	Ta	16.94 ± 0.94	14.07 ± 0.09
11	Ta	15.30 ± 1.04	14.82 ± 0.08	Ti	15.64 ± 0.79	5.39 ± 0.07
12	Ti	13.90 ± 0.86	5.95 ± 0.13	Ta	14.25 ± 1.10	14.52 ± 0.03
13	Ta	12.40 ± 1.21	14.51 ± 0.11	Ti	12.78 ± 0.92	5.55 ± 0.07
14	Ti	10.77 ± 1.01	5.07 ± 0.07	Ta	11.18 ± 1.28	14.64 ± 0.06
15	Ta	8.97 ± 1.41	14.09 ± 0.9	Ti	9.43 ± 1.07	5.31 ± 0.02
16	Ti	6.92 ± 1.18	5.17 ± 0.05	Ta	7.44 ± 1.50	14.18 ± 0.06
17	Ta	4.39 ± 1.68	13.76 ± 0.15	Ti	5.06 ± 1.27	5.39 ± 0.03
18	Ti	1.39 ± 1.43	5.85 ± 0.08	Ta	1.96 ± 1.83	14.41 ± 0.15

the isomeric pair ^{182}Re^{m,g} was calculated from the present experimental data. The isomeric ratio of a specific pair is sensitive to the spin difference between their involved levels [9,10]. Its dependence on the projectile energy was presented as well as its role in the reaction mechanisms.

The nuclear reaction modeling codes, TALYS-1.9 [11] and EMPIRE 3.2.3 [12], were used to calculate the investigated excitation functions. The theoretical excitation functions were compared to the experimental results in order to test the reliability of the codes. In this work, the default parameters were used in TALYS calculations in the form of the TENDL-2019 nuclear data library while in EMPIRE calculations, different sets of modeling parameters for equilibrium and preequilibrium reactions were used. The theoretical isomeric cross-section ratio of the isomeric pair ^{182}Re^{m,g} was also calculated utilizing the TENDL-2019 library as well as different modeling parameters of EMPIRE, especially the level density parameter.

II. EXPERIMENTAL TECHNIQUES

Cross sections were measured utilizing the well-known stacked-foil activation technique, which involves irradiation of a set of thin foils and identification of the residual radioactive products. This technique is effective in inspecting low-yield reaction products and closely spaced and/or low-lying isomeric states, such that their lifetimes are not too short. The details of the activation technique have been described over the years in many publications [13–15]. Here we give only the basic attributes of the present measurements.

A. Samples and irradiation

High-purity natural tantalum foils 99.98% (8.6 μm thick) and natural titanium foils 99.5% (12 μm thick) supplied by Goodfellow, England were activated using the stacked-foils technique. Two stacks of tantalum foils sandwiched with titanium foils were irradiated individually. Each stack consisted of nine natural tantalum target foils and nine interleaved titanium foils. The titanium foils served as recoil catchers for the radioactive products, ^{3}He beam monitors, as well as beam energy degraders. The two stacks were irradiated in a Faraday-like cup target holder equipped with a beam collimator (slot diameter equals 10 mm) and a secondary electron suppressor. The beam effective diameter on the target was about 5 mm. The target holder was also equipped with a current integrator to determine the integrated charge of the beam. Table I presents the arrangement of target foils in each stack and their measured thicknesses in the form of areal densities. Uncertainty in the areal density of each foil was calculated from dimensions and masses uncertainties.

For each stack, the intensity of the beam was maintained as a constant value during irradiation. The irradiations were performed, for 1 h for each stack, at the external beam of the MGC-20E cyclotron of ATOMKI, Debrecen, Hungary. Each stack was irradiated using a ^{3}He-particle beam of about 100 nA current and incident energy of about 27 MeV. The initial beam parameters for each irradiation, incident energy and particle flux, were derived from the accelerator setting and the integrated charge in the Faraday cup. These measurements were verified and improved by evaluating the excitation functions of the monitor reactions to remeasure the actual beam energy and current during the irradiation. The IAEA recommended cross-section data of the monitor reaction ^{nat}Ti(^{3}He, x)^{48}V [16] were used, and a good agreement between the present and the recommended data was obtained and displayed in (Fig. 1).

B. Measurement of radioactivity

Residual activities in the irradiated target and monitor foils were measured, nondestructively (without chemical

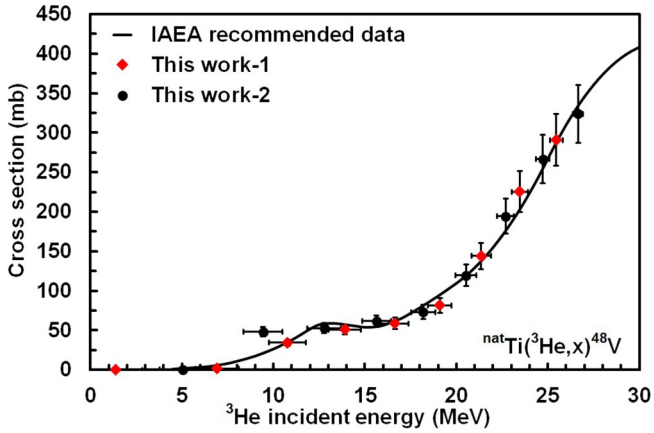

FIG. 1. Monitor reaction excitation function for ^{nat}Ta activation by ^{3}He particle.

processes), using two high-resolution gamma-ray spectrometers. They both consisted of a lead-shielded HPGe "CANBERRA" detector of resolution 2 keV at the 1333-keV energy line, equipped with a multichannel analyzer and an acquisition/analysis software. The detectors' efficiencies were calculated for different source to detector distances using a set of gamma-ray standard sources that cover the entire gamma-energy domain. The samples were measured at different and large enough sample to detector distances to reduce dead times and avoid pile-up effects. The target foils were measured three times. The first two measurements started on the same day of irradiation while a third long measurement started three days after end of bombardment (EOB). Measurements of the monitor foils for each experiment were started more than two weeks after EOB. This technique of monitor measurement ensures total decay of the short-lived radionuclide ^{48}Sc which has the same gamma lines of the interested longer-lived nuclei ^{48}V. The collected spectra of target and monitor foils were analyzed using the gamma-spectrum analysis program FGM [17] and the gamma-analysis software from Canberra, GENIE 2000 [18]. The produced radionuclides were analyzed by their intense, different, and independent gamma lines if available. This ensures the reliability of the calculated activities as well as the utilized decay data. When there were no independent gamma lines, either suitable cooling times or solving differential decay equations were used to calculate the independent activities, depending on the half-lives of the interfered radionuclides.

C. Calculation of cross sections and uncertainties

The production cross section of any radionuclide was estimated using its calculated activity, beam, and target characteristics using the activation formula. The formula could be expressed as

$$A^{0}_{\mathrm{EOB}} = \sigma\, n\, \varphi\, [1 - \exp(-\lambda t_i)]\ (Bq), \qquad (1)$$

where A^{0}_{EOB} is the produced activity (Bq) of a given radionuclide at EOB, σ is its production cross section (cm^2), n is the surface density of the target foil, φ is the beam current (particle/sec), λ is the decay constant of the interested radionuclide, t_i is the irradiation time. The EOB activity could be expressed as

$$A^{0}_{\mathrm{EOB}} = C_\gamma t_r \lambda / t_l \varepsilon_\gamma I_\gamma e^{-\lambda t_c}[1 - \exp(-\lambda t_r)]\ (Bq), \qquad (2)$$

where C_γ is the net count area of the photopeak at certain gamma energy in the interested radioisotope decay scheme, ε_γ is the detector efficiency at this gamma line, I_γ is the absolute intensity of this gamma line and t_r, t_l, and t_c are the measurement real, live times, and cooling time after EOB.

Nuclear decay data and reaction characteristics were taken in general from the NuDat2.8 database [5]. However, due to a shortage of nuclear decay data in the region of interest, we derived some decay data, for comparison and calculation, from the databases LUND [19], live chart of nuclides from Nuclear Data Service NDS, IAEA [20], Japanese nuclear data library [21], and table of gamma rays of Nuclear Data Center at Korean Atomic Energy Research Institute (KAERI) [22]. Nuclear structure and decay data of the investigated radionuclides were also checked via the nuclear data sheet articles [23–27] individually. Whenever a nuclear database other than Nudat2.8 was used in the calculations, it was mentioned in the text. Table II presents the decay data of the investigated radioisotopes, their producing nuclear reactions, and reaction kinematics.

Energy degradation along the foils was calculated by the computer program SRIM-2013 based on polynomial approximations for the stopping power and range of ^{3}He energetic particles in natural tantalum [28]. The incident energies (median energy in the first foil) were estimated as 26.41 ± 0.3 MeV for the first stack and 26.65 ± 0.29 for the second stack. The uncertainty on the median energy in each foil is increasing along with the stack foils due to the cumulative effect of energy spread and the variations in foil thicknesses. It reached a maximum value of ± 1.43 MeV at the last foil of the first stack and ± 1.41 at the last foil of the second stack.

The experimental uncertainties were calculated assuming linear contributions from the independent processes by the standard method [29]—from the square root of quadratically summed relative uncertainties. The following individual uncertainties were considered: the number of bombarding particles (7%), determination of the thickness of each foil (3%), nuclear decay data (3%), absolute detector efficiency (7%), and peak area (10%). The total experimental uncertainties on the cross-section values were approximately 15%. In some cases, they were even higher.

III. NUCLEAR MODEL CALCULATIONS

A. TALYS1.9

TALYS is a nuclear reaction code that works at the UNIX platform created at NRG, Petten, the Netherlands, and CEA, Bruyères-le-Châtel, France. It provides a complete simulation of nuclear reactions over a wide energy range, 1 keV–200 MeV, through a combination of different reliable nuclear models [30]. The reference input parameters library (RIPL-3) is included in the TALYS database [31]. The coupled-channels CC-code ECIS06 [32] is used in TALYS as a subroutine for both optical model and direct reaction. The default optical model potentials (OMPs), used in calculations, are the

TABLE II. Decay data and contributing reactions of the products of ^{181}Ta + ^{3}He.

Product	Contributing reaction	E_{th} (MeV)	Decay mode (%)	Half-life	E_γ (keV)	I_γ (%)
^{181}Re	(^{3}He, 3n)	11.4	EC + β^+ (100)	19.9 h	360.7	20
					365.5	56
					639	6.4
					953.6	3.6
^{182}Re^{g}	(^{3}He, 2n)	4.28	EC + β^+ (100)	64.2 h	169.15	11.4
					256.45	9.5
					286.56	7.1
					1427.3	9.8
^{182}Re^{m}	(^{3}He, 2n)	4.34	EC + β^+ (100)	14.14 h	1121.4	32
					1189.2	15.1
					1221.5	25
^{178}Ta^{A}	(^{3}He, α2n)	1.5	EC + β^+ (100)	2.36 h	213.44[a]	81.4[a]
	(^{3}He, 4n2p)	30.27				
					325.56[a]	94.1[a]
					426.38[a]	
						97[a]
^{180}Ta^{g}	(^{3}He, α)	0	EC (85)	8.15 h	93.32	4.5
	(^{3}He, 2n2p)	15.55	β^- (15)		103.6	0.87

[a]Gamma lines are taken from the LUND database because they were not found in NuDat2.8.

local and global parametrizations for neutrons and protons of Koning and Delaroche (2003) [33]. For pre-equilibrium nucleon emission, TALYS used a two-component exciton model based on the OMP of Koning and Delaroche [33,34]. For equilibrium particle emission, TALYS used the complete Hauser-Feshbach formalism including width fluctuation corrections (WFCs) [35]. For level density calculations TALYS introduced six models. Three of them are phenomenological models: Fermi gas and constant temperature Fermi gas model (FGM and CTFGM), back-shifted Fermi gas model (BSFGM), and generalized superfluid model (GSFM). The other models are tabulated level densities derived from different microscopic level densities. The six models are denoted Idmodel 1–6 in TALYS-code parameters.

In this paper, the nuclear data library TANDL-2019 based on calculations with the TALYS-1.9 code, using sets of parameters selected by the TALYS team, was used for all cross-section calculations.

B. EMPIRE 3.2.3

EMPIRE 3.2.3; an updated version of EMPIRE [12], is a modular system of nuclear reaction codes designed for simulation of nuclear reactions by various theoretical nuclear codes. It works at both UNIX and WINDOWS platforms and delivers a complete description of nuclear reactions over a broad range of energies and incident particles [36]. It consists of several FORTRAN-based nuclear codes, input parameter libraries based mainly on RIPL-2, 3 [37,31], and experimental data library EXFOR. The direct nuclear reactions are described by two generalized optical model codes: the coupled-channel (CC) and distorted wave Born approximation (DWBA) code ECIS06 and the coupled-channel code OPTMAN. The pre-equilibrium nuclear reactions are described by quantum mechanical and/or phenomenological models. The quantum pre-equilibrium models are the multistep direct (MSD) and the multistep compound codes. The phenomenological pre-equilibrium models are the classical exciton model PCROSS and the Monte Carlo simulation model DDHMS. The equilibrium nuclear reactions are described by the full-featured Hauser-Feshbach theory combined with γ cascade and width fluctuation correction.

Only one optical model parameter (OMP) set for ^{3}He interaction with tantalum was found in the RIPL-3 and used in our calculations. In the present work, pre-equilibrium processes were calculated by the PCROSS model using different values of the mean free path parameter ranging from $k_{mfp} = 0$ (where PCROSS is not included) and $k_{mfp} = 3$ and different values of the MAXHOL parameter ranging from $MH = 0.1$ (equivalent to lowest pre-equilibrium contribution) and $MH = 1.5$ (equivalent to highest pre-equilibrium contribution). Nuclear level densities (NLDs) are described in EMPIRE3.2.3 by five models which are included in the RIPL. These models are the enhanced generalized superfluid model (EGSM), the generalized superfluid model (GSM), the Gilbert-Cameron model (GCM), the Hartree-Fock-Bogoliubov microscopic model (HFBM), and the fifth model is taken from the EMPIRE 2.18 version. Various combinations of NLD models and PCROSS parameters were used in the present calculations. Whenever EMPIRE could reproduce the experimental data, the best combination as well as the default parameter excitation functions were introduced. But when EMPIRE couldn't reproduce the experimental data for all combinations, EMPIRE excitation functions were presented as a gray region instead of discrete curves. This region represents the expectation area which lies between the minimum and maximum predicted excitation functions by the different parameter combinations. EMPIRE produces two output files for nuclear reaction cross-section data. One of them contains the total reaction cross section of the investigated nuclides and the other contains full details including the isomeric cross sections. To calculate separate isomeric and

TABLE III. Numerical cross-section and isomeric cross-section values and uncertainties of the produced radionuclides.

	$\sigma \pm \Delta\sigma$ (mb)					Isomeric ratio
$E \pm \Delta E$ (MeV)	^{181}Re	^{182}Re^{g}	^{182}Re^{m}	^{187}Ta^{A}	^{180}Ta^{g}	^{182}Re$^{m/g}$
26.41 ± 0.39	485.4 ± 57.2	11.44 ± 1.32	9.44 ± 1.09	1.36 ± 0.21	24.43 ± 4.77	0.83 ± 0.17
25.69 ± 0.43	491.2 ± 58.5	10.31 ± 0.76	9.71 ± 0.88	1.12 ± 0.22	29.20 ± 6.20	0.94 ± 0.17
24.48 ± 0.50	499.6 ± 60.6	10.14 ± 1.22	8.74 ± 1.05	0.77 ± 0.17	31.40 ± 5.39	0.86 ± 0.19
23.72 ± 0.55	462.4 ± 53.9	10.14 ± 0.77	9.62 ± 1.08	0.65 ± 0.12	33.07 ± 6.20	0.95 ± 0.19
22.43 ± 0.62	362.2 ± 43.4	10.37 ± 1.30	8.64 ± 1.08	0.33 ± 0.08	29.96 ± 5.38	0.83 ± 0.19
21.62 ± 0.67	273.4 ± 33.8	10.01 ± 0.64	9.30 ± 0.85	0.24 ± 0.08	22.04 ± 4.13	0.93 ± 0.20
20.25 ± 0.75	151.7 ± 20.0	8.57 ± 1.15	7.47 ± 1.00	0.11 ± 0.02	13.73 ± 3.51	0.87 ± 0.21
19.38 ± 0.80	88.1 ± 13.2	6.87 ± 0.58	6.26 ± 0.60		13.68 ± 3.75	0.91 ± 0.22
17.89 ± 0.89	24.6 ± 4.60	3.09 ± 0.55	4.09 ± 0.73		5.85 ± 1.60	1.32 ± 0.30
16.94 ± 0.94	8.9 ± 1.40	0.89 ± 0.10	2.61 ± 0.31			2.94 ± 0.41
15.30 ± 1.04	1.1 ± 0.20		0.55 ± 0.19			

ground state cross sections, the isomeric cross section was subtracted from the total reaction cross section of a certain radionuclide.

IV. RESULTS AND DISCUSSION

The measured experimental cross sections of the nuclear reactions (^{3}He, $2n$) ^{182}Re^{m,g}, (^{3}He, $3n$) ^{181}Re, (^{3}He, x) ^{180}Ta^{g}, and (^{3}He, x) ^{178}Ta^{A} in addition to the calculated isomeric cross-section ratio of the isomeric pair ^{182}Re^{m,g} are shown in Figs. 4–9. Available literature data as well as theoretically calculated cross sections, based on TENDL-2019 and EMPIRE 3.2.3, are also presented in those figures. The (^{3}He, n) ^{183}Re channel couldn't be observed in the present measurements. That is, partially, because of low cross-section values of the (^{3}He, n) channel in general, as well as the long half-life of the product ^{183}Re, whereas we limited the present measurement plan to short-lived radionuclides due to lack of detectors at the measurement time. Numerical cross-section values and cross-section uncertainties are presented in Table III for the investigated radioisotopes as well as the isomeric cross-section ratio of the isomeric pair ^{182}Re^{m,g}.

A. ^{181}Ta(^{3}He, $3n$) ^{181}Re

^{181}Re ($T_{1/2} = 19.9$ h, $J^{\pi} = 5/2^{+}$) decays by 100% EC + β^{+} to ^{181}W with an extremely small β^{+} branch (0.004%). ^{181}Re is formed only via the reaction (^{3}He, $3n$) and hence the production cross section is a direct process. Four strong gamma lines were found in the different nuclear structure databases: ($E_\gamma = 360.7$ keV, $I_\gamma = 20\%$), ($E_\gamma = 365.5$ keV, $I_\gamma = 56\%$), ($E_\gamma = 639$ keV, $I_\gamma = 6.4\%$), and ($E_\gamma = 953.6$ keV, $I_\gamma = 3.6\%$) [5]. There is a small difference in the values of gamma energies/intensities between the different databases [5,19–22,24,38].

Figure 2 displays one of the generated spectra showing the list of gamma lines from the decay of the produced radionuclides. In the present cross-section calculations for this radionuclide, the nuclear decay data were taken from [5]. For each target, the measured EOB activities, i.e., cross sections, of the radionuclide ^{181}Re using the different gamma lines were consistent except that delivered by the 360-keV gamma line. The measured radioactivity using this gamma line was about half the values of that delivered by the other lines.

1. Experimental intensity of the 360.7-keV gamma ray in ^{181}Re decay

We followed the radioactive decay of ^{181}Re for each target using the different gamma lines to estimate its half-life and activity. Figure 3 shows that half-life values derived from the different gamma lines are almost identical and close to the reported value in the different nuclear decay databases. Despite this, the calculated EOB activity for the 360-keV line was found to be approximately half the value of the other lines. The slight difference between the experimental half-lives and the reported value in the decay databases is due to the low number of target measurements and doesn't distort the conclusion.

According to the activation formula, we assumed that the inconsistency in the measured activity is due to an error in the reported gamma intensity of the 360-keV line. Its intensity in the different databases ranges from 19.76% to 21.11%. By a simple mathematical analysis and using the measured EOB activity from the different gamma lines, we can estimate an

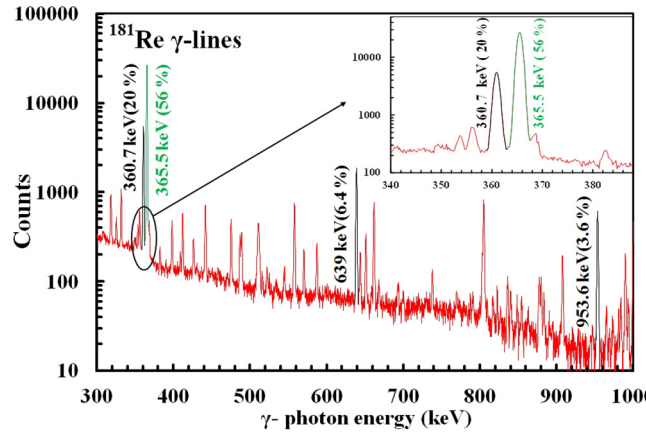

FIG. 2. Part of a spectrum showing ^{181}Re gamma lines.

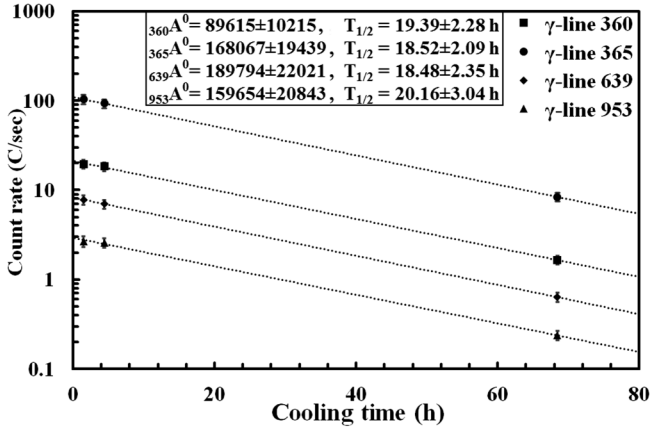

FIG. 3. Experimental decay curves of ^{181}Re using its different gamma lines measured in one target foil.

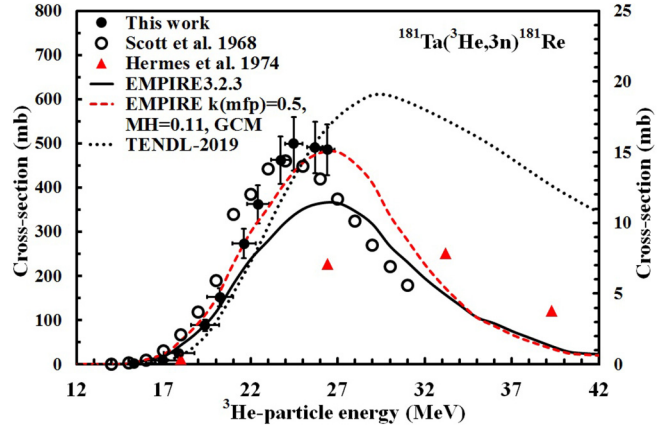

FIG. 4. Theoretical and experimental excitation functions of the ^{181}Ta(^{3}He, $3n$) ^{181}Re reaction. TENDL-2019 excitation function is represented on the secondary axis.

experimental intensity for the 360-keV energy line as follows:

$$A^0_{\mathrm{EOB}} = \frac{C_{\gamma 1} t_r \lambda}{t_l \varepsilon_{\gamma 1} I_{\gamma 1} e^{-\lambda t_c}[1 - \exp(-\lambda t_r)]} = \frac{C_{\gamma 2} t_r \lambda}{t_l \varepsilon_{\gamma 2} I_{\gamma 2} e^{-\lambda t_c}[1 - \exp(-\lambda t_r)]}, \quad (3)$$

where γ_1 and γ_2 subscripts identify that the quantities refer to the 360-keV gamma line and the other lines respectively. Since all the terms are identical except the net count areas, energy-line efficiencies, and intensities, then

$$I_{\gamma 1}/I_{\gamma 2} = C_{\gamma 1}\epsilon_{\gamma 2}/C_{\gamma 2}\varepsilon_{\gamma 1}. \quad (4)$$

From this formula, the intensity of the 360-keV gamma line was estimated many times using the other mentioned lines. About 11 targets were used in the measurements such that each target delivered nine values for the intensity of that line. Thus, about 99 estimated values were used to derive an average experimental value for the 360-keV line intensity. Table IV displays the present average experimental intensity in addition to the reported intensities in the different nuclear structure databases for the 360-keV gamma line. Finally, it remains to emphasize that we do not doubt the reported half-life values of ^{181}Re, we doubt only the reported intensities of the 360-keV gamma line in the ^{181}Re decay scheme. It is worth noting that we faced this problem when studying proton activation of tungsten in a paper not yet published and that we are working on measuring the intensity of this line with high accuracy.

TABLE IV. Experimental values for ^{181}Re half-life and its 360-keV gamma-line intensity in comparison with the reported values in the different databases.

Database	Half-life (h)	E_γ (keV)	I_γ (%)
NuDat2.8 [5]	19.9 ± 0.7	360.7 ± 3	20 ± 4
LUND [19]	19.9 ± 0.7	360.7 ± 0.11	20 ± 4
NDS [20]	19.9 ± 0.7	360.7 ± 3	20 ± 4
JAEA [21]	19.9 ± 0.7	360.7	19.76
KAEIR [22]	19.9 ± 0.7	360.7	21.107
This work	19.23 ± 2.04	360.7	10.45 ± 1.78

The present excitation function and those found in the literature were compared and are displayed, as well as the theoretical calculations (Fig. 4). The excitation function shows a peak of about 500 mb at 24.5 MeV. The present experimental data are in good agreement with Scott *et al.* [6]. The high energy tail of the excitation function of Hermes *et al.* [7] has the same trend as the data of Scott *et al.* [6]. There are two cross-section data points from [7] in our energy range. The lowest energy data point at 18 MeV corresponds to the last foil in their irradiated stack. The cross-section value at that point is lower than the present data; probably because of the error in the energy determination as a result of irradiation with high energy ^{3}He particles. The other data point at 26.4 MeV has a lower cross-section value than the present data by 60%. This data point corresponds to the additional irradiation of single tantalum foil by a Van de Graff. We couldn't recognize a reason for this disagreement. It should be noted that the displayed literature data in Fig. 4 represent adjusted data according to the present intensity of the 365-keV gamma line.

The theoretical excitation function delivered by TENDL-2019 (represented on the secondary axis in Fig. 4) approximately has the same trend as the experimental excitation function. The code delivers lower cross-section data than the present data with a maximum cross-section value of 19 mb around 30 MeV, about 5 MeV farther than the present data.

For the EMPIRE 3.2.3 excitation function, the calculations were performed for several combinations of equilibrium and pre-equilibrium parameters included in the code. For all combinations, the code predicts the same trend of the experimental excitation function. The best matching was achieved by using the phenomenological refitted Gilbert and Cameron level density model (GCM) in combination with the PCROSS parameters $k_{\mathrm{mfp}} = 0.51$ and $MH = 0.1$. This combination indicates a low contribution from the pre-equilibrium mechanism and domination of the compound nucleus in our energy range. This result was observed in the previous work by Scott *et al.* [6] where they concluded that (^{3}He, xn); $x > 1$,

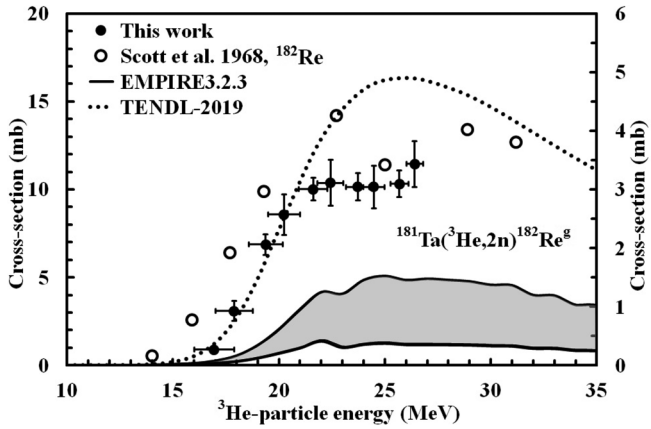

FIG. 5. Excitation functions of the ^{181}Ta(^{3}He, $2n$)^{182}Re^{g} reaction. TENDL-2019 excitation function is represented on the secondary axis.

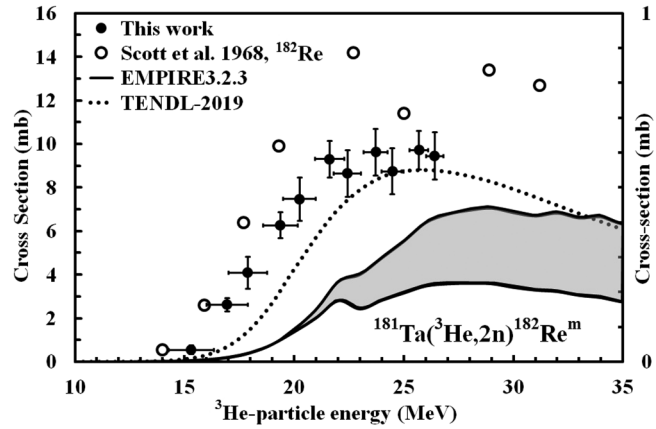

FIG. 6. Excitation functions of the ^{181}Ta(^{3}He, $2n$)^{182}Re^{m} reaction. TENDL-2019 excitation function is represented on the secondary axis.

reactions proceed predominantly by equilibrium emission. At higher energies, the pre-equilibrium mechanism is expected to dominate producing the high energy tail. Figure 4 shows EMPIRE excitation functions both for suitable and default input parameters.

B. ^{181}Ta(^{3}He, $2n$)^{182}Re^{m,g}

The ground and isomeric states of the radionuclide ^{182}Re are too close. With ($T_{1/2} = 64.2$ h, $J^{\pi} = 7^{+}$) for the ground state and ($T_{1/2} = 14.14$ h, $J^{\pi} = 2^{+}$) for the isomeric state, both decay by 100% EC + β^{+} to ^{182}W [5]. The half-life of the isomeric state in the other nuclear databases [19,21,22] is 12.7 h. However, the value adopted by the NuDat 2.8 [5] corresponds to recent measurements. There are many gamma lines in their decay schemes but, unfortunately, the strongest lines are common to them. To measure their cross sections individually we first measured the ground state cross section using the uncommon gamma lines ($E_{\gamma} =$ 169.15 keV, $I_{\gamma} = 11.4\%$), ($E_{\gamma} = 256.45$ keV, $I_{\gamma} = 9.5\%$), ($E_{\gamma} = 286.56$ keV, $I_{\gamma} = 7.1\%$), and ($E_{\gamma} = 1427.3$ keV, $I_{\gamma} =$ 9.8%). Then, using the ground state activity and the common lines ($E_{\gamma} = 1121.4$ keV, $I_{\gamma} = 32\%$), ($E_{\gamma} = 1189.2$ keV, $I_{\gamma} =$ 15.1%), and ($E_{\gamma} = 1221.5$ keV, $I_{\gamma} = 25\%$), the isomeric state cross section was determined. Production cross sections of both ^{182}Re^{m,g} are direct processes since there is no isomeric transition and they are only produced from the reaction channel ^{181}Ta(^{3}He, $2n$).

The two experimental excitation functions started at about 15 MeV and formed a plateau in the energy range 21–26 MeV (Figs. 5 and 6). Scott *et al.* [6] presented only one cross-section data set for the channel (^{3}He, $2n$) without the determination of the individual cross sections for isomeric and ground states. Their data are higher than both the present ground and isomeric state cross-section data by about 30–40% and lower than their sum. However, the present experimental excitation functions and the literature one has the same trend.

The TENDL-2019 nuclear data library presents very low cross sections concerning the present data. The calculated cross-section values by TENDL-2019 for the ground state are ten times larger than that calculated for the isomeric state, probably due to the difference in their spin. The measured experimental data, however, do not confirm this big difference. Instead, the experimental cross-section values for both the ground and the isomeric states are comparable. The ground state cross-section values are slightly higher, over 19 MeV.

Ground and isomeric state excitation functions predicted by EMPIRE code for all parameter combinations have the same trend of the experimental data. The code excitation functions underestimate the experimental data for the isomeric pair. Ground state predicted excitation functions reach their maximum values at 25 MeV, earlier than isomeric state predicted excitation functions that reach their maximum values at 29 MeV.

Unlike experimental and TENDL-predicted data, the isomeric cross-section values predicted by EMPIRE are two to three times higher than EMPIRE ground state values. For both ground and isomeric predicted excitation functions, there is a small peak around 22 MeV for all combinations. This peak is located just before the Coulomb barrier at $E_{c} = 22.7$ MeV. It is then probably a result of the Coulomb barrier. The same trend is not confirmed clearly by the experimental data.

Experimental and theoretical cross-section data for the isomeric pair exhibit a broad peak and high energy tail which indicates the domination of the pre-equilibrium reaction mechanism. This trend is obvious in the experimental and theoretical data, especially over 20 MeV. This result could be checked by using the energy dependence of the isomeric cross-section ratio. For this purpose, an experimental as well as a theoretical isomeric cross-section ratio was plotted as a function of the ^{3}He-beam energy (Fig. 7). Below 19 MeV, the experimental ratio decreases with energy from 3 at 17 MeV to 1 at 19 MeV, i.e., the isomeric cross section is greater than the higher-spin ground state cross section, but the ground state value increases with energy. This indicates that the contribution from the compound reaction mechanism slowly increases with energy but does not dominate the low energy region. Over 19 MeV up to the end of our energy range, the ratio settles down to 1. So, the reaction doesn't boost the production of the high-spin ground state at the broad peak

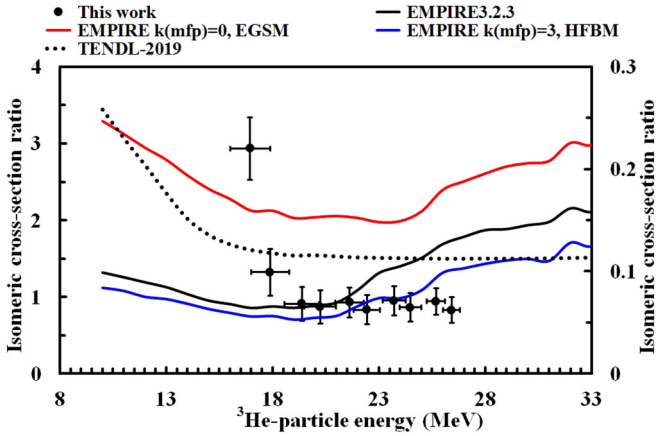

FIG. 7. Isomeric cross-section ratio of the ^{181}Ta(^{3}He, $2n$) ^{182}Re^{m,g} reaction. TENDL-2019 excitation function is represented on the secondary axis.

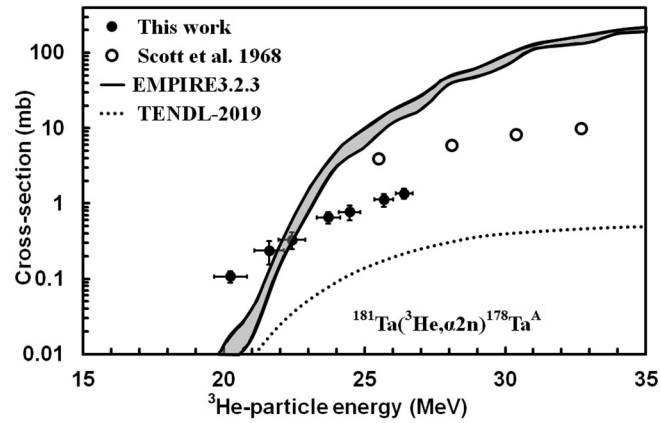

FIG. 8. Excitation functions of the ^{181}Ta(^{3}He, $\alpha 2n$) ^{178}Ta^A reaction. TALYS 1.9 code excitation function is represented on the secondary axis.

and the high energy tail. This features the domination of the pre-equilibrium reaction mechanism.

Figure 7 shows also the theoretical isomeric cross-section ratio derived from TENDL-2019 (presented on the secondary axis), and from EMPIRE using different level density models and PCROSS parameters. TENDL calculated isomeric ratios have the same trend as the experimental ratio with lower values. Below 15 MeV the calculated isomeric ratio decreases with energy from 0.26 at 10 MeV to 0.14 at 15 MeV, i.e., the higher spin ground state production rate increases with energy and is very favorable. Then the calculated ratio stabilizes at 0.11 for the whole energy range. This indicates the domination of the compound nucleus mechanism at lower energies with a large contribution from the pre-equilibrium mechanism over 15 MeV.

EMPIRE calculated isomeric ratios, on the other hand, differ from the trend of the experimental data. The ratio decreases with energy up to about 21 MeV then increases with energy for all combinations of the code parameters including level density models and PCROSS parameters. The ratio magnitude changes with both the level density models and the mean free path parameter of the PCROSS model. As the mean free path parameter increases from $k_{\rm mfp} = 0$ to $k_{\rm mfp} = 3$, i.e., the pre-equilibrium mechanism contribution increases, the EMPIRE calculated isomeric ratio is more consistent with the experimental data in the energy range 20–25 MeV.

C. ^{181}Ta(^{3}He, $\alpha 2n$) ^{178}Ta^A

The radionuclide ^{178}Ta has two close states, both adopted as ground states in the different nuclear databases individually. There are no indications to adopt one of them as the ground state [5]. Hence, we labeled them as the A state ($T_{1/2} = 2.36$ h, $J^\pi = 7^-$) and, the B state ($T_{1/2} = 9.31$ min, $J^\pi = 1^+$). The two states decay by 100% EC + β^+ to ^{178}Hf. There are two other short-lived isomeric states (half-lives in milliseconds) that decay by 100% IT to the A state. Therefore, the production of this state is a cumulative process.

Here we measured the cumulative cross section of the A state after total decay of the isomeric states, and even after total decay of the B state to prevent the interference in the common gamma lines. There were no gamma lines in the NuDat database for the A-state decay so we used the LUND database decay data in the cross-section measurements. The gamma lines ($E_\gamma = 213.44$ keV, $I_\gamma = 81.4\%$), ($E_\gamma = 325.56$ keV, $I_\gamma = 94.1\%$), and ($E_\gamma = 426.38$ keV, $I_\gamma = 97\%$) were used in the measurements.

The present excitation function started at 20.25 MeV and reached a maximum value of 1.36 mb at the end of our energy range. The direct production of ^{178}Ta^A comes through the channel (^{3}He, $2p4n$), $E_{\rm th} = 30.3$ MeV. However, the experimental threshold at 20 MeV (Fig. 8) indicates the emission of clusters through one of the channels (^{3}He, $\alpha 2n$), (^{3}He, $2t$), and (^{3}He,ndt) with threshold energies 1.5, 13, and 19.4 MeV respectively.

Scott *et al.* [6] presented four cross-section data points in the energy range 25.5–32.7 MeV. They used the 213.4-keV gamma line in the cross-section measurement with higher intensity than the recently reported value. We normalized their data according to the LUND database. Their data after normalization are three times higher than the present data with the same trend.

TENDL-2019 predicts very low cross sections with respect to the present data. However, it generates the same trend as the experimental excitation functions.

EMPIRE code excitation functions for the various parameter combinations have the same trend of the experimental data and overestimate them after 22 MeV.

D. ^{181}Ta(^{3}He, α) ^{180}Ta^g

The radionuclide ^{180}Ta has a ground state with ($T_{1/2} = 8.15$ h, $J^\pi = 1^+$) decays by two modes: β^- (15%) to ^{180}W and EC + β^+ (85%) to ^{180}Hf. The strong gamma line in its decay scheme, ($E_\gamma = 93.32$ keV, $I_\gamma = 4.51\%$), is unfortunately common with an energy line in the decay scheme of ^{178}Ta. Therefore, the low-intensity gamma line ($E_\gamma = 103.6$ keV, $I_\gamma = 0.87\%$) was used for the cross-section measurements. The cross-section data were then confirmed by using the common gamma line (93.32 keV) after subtracting the activity of

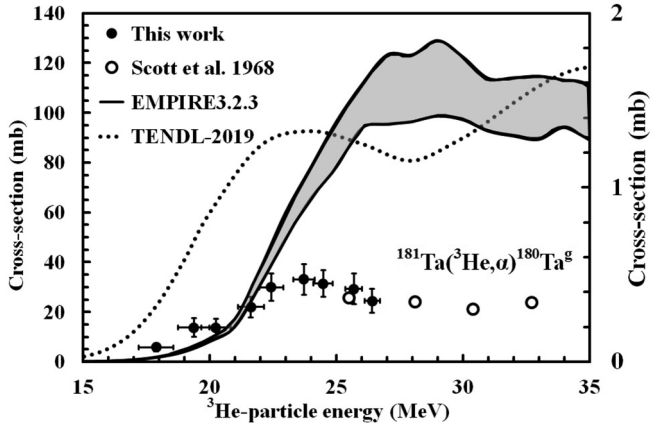

FIG. 9. Excitation functions of the ^{181}Ta(^{3}He, α) ^{180}Ta^{g} reaction. TALYS 1.9 code excitation function is represented on the secondary axis.

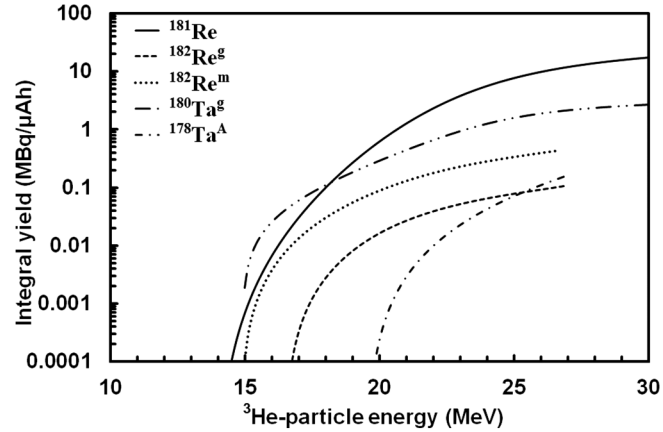

FIG. 10. Calculated integral yields for the nuclear reactions ^{181}Ta(^{3}He, x) ^{181}Re, ^{182}Re^{m,g} and ^{181}Ta(^{3}He, x) ^{178}Ta^{A}, ^{180}Ta^{g}.

the radionuclide ^{178}Ta. The production of ^{180}Ta^{g} is a direct process only from the channel (^{3}He,α).

The experimental excitation function shows a peak with a 33-mb cross-section maximum value around 24 MeV (Fig. 9). The low intensity of the investigated gamma line (103.6 keV) and the activity subtraction process resulted in high uncertainties in the cross-section values. The experimental threshold of the excitation function at about 18 MeV may indicate the contribution from the individual-particle emission channel (^{3}He, $2p2n$), $E_{\text{th}} = 15.5$ MeV. The formation rate increases over 21 MeV probably due to the effect of the Coulomb barrier, $E_c = 22.7$ MeV.

Scott *et al.* [6] measured the cross-section data for this reaction in the energy range 25.5–33 MeV. They stated that they used the gamma line ($E_\gamma = 103$ keV, $I_\gamma = 4.4\%$) for the identification of this radionuclide. The intensity they introduced for this line is more than five times the recently reported intensity. There is another gamma line with energy 93.3 keV close to the 103-keV line that has the same intensity they introduced for it. As they used an 11.6-cm^3 Ge(Li) detector [in a few cases they used 7.6 cm × 7.6 cm NaI(Tl) crystal] in the activity measurements, we hence suggested that they identified the radionuclide ^{180}Ta^{g} by the gamma line 93.3 keV and not by the 103-keV line. After normalization of their cross-section data according to the recent intensity of the 93.3-keV gamma line, their data are in good consistency with the present data. Their data confirmed the peak around 25 MeV and suggested a plateau region with a second peak at some energy higher than 30 MeV.

TENDL-2019 predicts very low cross sections with respect to the experimental data. It generates the same trend of the experimental excitation function with two peaks at energies 24 and 35 MeV.

EMPIRE calculated excitation functions, using the various parameter combinations, have the same trend of the experimental data. However, the code predicts higher cross-section values than the experimental data after 20 MeV. The code also predicts a higher production rate after ^{3}He-particle energy 21 MeV than before this energy. This is the same trend as the experimental data which probably is a result of the Coulomb barrier. The code excitation function then forms a peak around 26 MeV followed by a semiplateau region.

V. INTEGRAL YIELD

Integral yields for the nuclear reactions ^{181}Ta(^{3}He, x) ^{181}Re, ^{182}Re^{m,g}, ^{178}Ta^{A}, and ^{180}Ta^{g} were estimated from the present experimental excitation functions and the stopping power/range of ^{3}He in ^{nat}Ta over the energy range from threshold up to 27 MeV (Fig. 10). The stopping power and range of ^{nat}Ta for ^{3}He particles were calculated using the SRIM code [28]. The yields were calculated in $MBq/\mu Ah$ and represent the formation of the investigated nuclei at an instantaneous irradiation time.

^{181}Re has the highest integral yield with $12\,MBq/\mu Ah$ over our energy range. The integral yields of the ground and isomeric states of ^{182}Re amount to 110 and $420\,kBq/\mu Ah$ respectively over the present energy range. The integral yield of the radionuclides ^{178}Ta^{A} and ^{180}Ta^{g} are 160 and $2150\,kBq/\mu Ah$ respectively over the present energy range. Although ^{181}Re and ^{178}Ta^{A} are medically relevant radionuclides, production through this route is worthless. They could be produced efficiently by proton, deuteron, and alpha-particle activation [39].

From a practical point of view, radioisotope production by ^{3}He-particle activation is only important whenever it is the only possible production route because of the high cost of the ^{3}He gas and consequently the lack of ^{3}He beam availability, in addition to the low beam intensity compared to other projectiles.

VI. CONCLUSION

Production of ^{182}Re^{m,g}, ^{181}Re, and ^{178}Ta^{A}, ^{180}Ta^{g} radioisotopes through the ^{3}He-induced nuclear reactions on natural tantalum were assessed from their threshold energies up to 27 MeV. Activation of tantalum by ^{3}He particles was performed using the stacked-foil technique at the external beam of the MGC-20E cyclotron of ATOMKI. The cross sections of the nuclear reactions ^{181}Ta(^{3}He, xn); $x = 2$, 3 and

^{181}Ta(^{3}He, $xn\alpha$); $x = 0$, 2 were measured and compared to the previous experimental literature data as well as theoretical data derived from TENDL-2019 nuclear data library and EMPIRE3.2.3 model. The literature data were normalized according to the present reported nuclear decay data.

The comparison between literature experimental data and the present data showed some discrepancies between them. Concerning ^{181}Re measurements, we found an inconsistency in the measured activity using the different gamma lines in its decay scheme. The activity measured using the 360.7-keV gamma line was found to be half the activity measured by the other lines. The decay of ^{181}Re was followed and consistency in the experimental half-lives measured by the different gamma lines was found. We assumed that this disagreement is due to an error in the reported intensity of the 360.7-keV gamma line. The present work assumed the new experimental intensity $I_\gamma = 10.45\%$ for the 360.7-keV gamma line to remove the inconsistency. The present experimental data are in good agreement with the data of Scott *et al.* (1968). Two cross-section data points from Hermes *et al.* (1974) in our energy range are lower than the present data probably due to an error in the energy determination. There are disagreements between the present excitation functions of the reactions ^{181}Ta(^{3}He, $2n$) ^{182}Re^{m,g}, and ^{181}Ta(^{3}He, $2n\alpha$) ^{178}Ta^{A} and those presented by Scott *et al.* (1968). For the (^{3}He, $2n$) channel, they presented only one cross-section data set instead of two sets for the ground and isomeric states. The present experimental excitation function of the reaction channel (^{3}He,α)^{180}Ta^{g} is in a good agreement with Scott *et al.* (1968) data. We suggested that they used the 93.3-keV gamma line in their cross-section measurements for this channel and not the line 103.6-keV line according to their reported gamma intensity. Excitation function behavior, broad peak and high energy tail, of the channel (^{3}He, $2n$) for the isomeric pair indicates domination of the pre-equilibrium mechanism over 19 MeV. The energy dependence of the experimentally calculated isomeric cross-section ratio confirmed this result.

The theoretical calculations by TENDL-2019 and EMPIRE 3.2.3 could reproduce only the trend of the experimental data by their default input parameters. The TENDL-2019 excitation functions underestimate the experimental data in all cases. On the other hand, the EMPIRE code accurately reproduces the experimental excitation function of the reaction channel (^{3}He, $3n$) with careful choice of the input parameters. The effective parameters in regenerating the excitation function of this channel indicate domination of the equilibrium mechanism in our energy range, a result concluded earlier by Scott *et al.* (1968). For the other nuclear reactions, the different combinations of the input parameters in PCROSS code and nuclear level density models reproduce only the trend of the excitation functions. For the theoretical isomeric cross-section ratio, TENDL-2019 and EMPIRE were used. Different sets of level density models and pre-equilibrium parameters were used in EMPIRE calculations. The ratio trend is reproduced well by the TENDL-2019 calculation, indicating pre-equilibrium domination just like the experimental result. However, the derived values are much lower than the experimental ratio. The EMPIRE code ratio, on the other hand, gave a different trend and magnitude from the experimental data.

ACKNOWLEDGMENTS

The authors appreciate gratefully Prof. A. Azzam for enlightening scientific discussion. This work was supported and funded by the Magyar Ösztöndíj Bizottság through the Balassi Intézet, Budapest, and Institute for Nuclear Research (ATOMKI), Debrecen, Hungarian Academy of Science under the Ref. No. MÖB/156-1/2013. The authors acknowledge the staff and operators of the Debrecen cyclotron for their help in performing irradiations.

[1] S. Sudár and S. M. Qaim, Cross sections for the formation of ^{195}Hg^{m,g}, ^{197}Hg^{m,g}, and ^{196}Au^{m,g} in α and ^{3}He-particle induced reactions on Pt: Effect of level density parameters on the calculated isomeric cross-section ratio, Phys. Rev. C **73**, 034613 (2006).

[2] M. Bonardi, F. Groppi, E. Persico, S. Manenti, K. Abbas, U. Holzwart, F. Simonelli, and Z. B. Alfassi, Excitation functions and yields for cyclotron production of radiorhenium via ^{nat}W(p,xn)$^{181-186g}$Re nuclear reactions and tests on the production of ^{186g}Re using enriched ^{186}W, Radiochim. Acta **99**, 1 (2011).

[3] F. Habashi, Historical introduction to refractory metals, Min. Proc. Ext. Met. Rev. **22**, 25 (2001).

[4] Tantalum-niobium international study center (T.I.C.), Lasne, Belgium. https://www.tanb.org/index/, 2020 (Accessed 20 April 2018).

[5] NuDat 2.8 database, national nuclear data center, brookhaven national laboratory, Upton, NY. https://www.nndc.bnl.gov/nudat2/, 2020 (Accessed 20 December 2019).

[6] N. E. Scott, J. W. Cobble, and P. J. Daly, A comparison of reactions induced by medium-energy ^{3}He and ^{4}He ions in favorable target nuclei, Nucl. Phys. A **119**, 131 (1968).

[7] F. Hermes, E. W. Jasper, H. E. Kurz, T. Mayer-Kuckuk, P. F. A. Goudsmit, and H. Arnold, Analysis for (Particle,xn) reactions on tantalum and gold. ^{181}Ta, ^{197}Au(^{3}He,xn) excitation functions and equilibrium statistical model analysis, Nucl. Phys. A **228**, 175 (1974).

[8] Y. Nagame, Y. Nakamura, M. Takahashi, K. Sueki, and H. Nakahara, Pre-equilibrium process in ^{3}He-induced reactions on ^{59}Co, ^{109}Ag, ^{181}Ta and ^{209}Bi, Nucl. Phys. A **486**, 77 (1988).

[9] S. M. Qaim, S. Sudár, and A. Fessler, Influence of reaction channel on the isomeric cross-section ratio, Radiochim. Acta **93**, 503 (2005).

[10] M. Al-Abyad, S. Sudár, M. N. H. Comsan, and S. M. Qaim, Cross sections and isomeric cross-section ratios in the interactions of fast neutrons with isotopes of mercury, Phys. Rev. C **73**, 064608 (2006).

[11] A. Koning, S. Hilaire, and S. Goriely, *TALYS-1.9: A Nuclear Reaction Program. User Manual* (*Nuclear Research and Consultancy Group (NRG)*, Petten, The Netherlands, 2017).

[12] M. Herman, R. Capote, M. Sin, A. Trkov, B. V. Carlson, P. Obložinský, C. M. Mattoon, H. Wienke, S. Hoblit, Y Cho, G. P. A. Nobre, V. A. Plujko, and V. Zerkin, EMPIRE-3.2 Malta. Modular system for nuclear reaction calculations and nuclear data evaluation, *User's Manual, IAEA Report INDC (NDS)-0603* (IAEA Nuclear Data Section, Vienna, 2013).

[13] F. Tárkányi, F. Ditrói, F. Szelecsényi, M. Sonck, and A. Hermanne, Measurement and evaluation of the excitation functions for alpha particle induced nuclear reactions on niobium, Nucl. Instrum. Methods Phys. Res. B **198**, 11 (2002).

[14] M. Al-Abyad, I. Spahn, and S. M. Qaim, Experimental studies and nuclear model calculations on proton induced reactions on manganese up to 45 MeV with reference to production of ^{55}Fe, ^{54}Mn and ^{51}Cr, Appl. Radiat. Isot. **68**, 2393 (2010).

[15] B. M. Ali, M. Al-Abyad, S. Kandil, A. H. M. Solieman, and F. Ditrói, Excitation functions of ^{3}He-particle-induced nuclear reactions on ^{103}Rh: Experimental and theoretical investigations, Eur. Phys. J. Plus **133**, 9 (2108).

[16] F. Tárkányi, S. Takács, K. Gul, A. Hermanne, M. G. Mustafa, M. Nortier, P. Obložinský, S. M. Qaim, B. Scholten, Yu. N. Shubin, and Y. Zhuang, Charged particle cross-section database for medical radioisotope production: Diagnostic radioisotopes and monitor reactions, *IAEA-TECDOC-1211* (IAEA, Vienna, 2001.

[17] G. Székely, FGM - A Flexible Gamma-spectrum analysis program for a small computer, Comput. Phys. Commun. **34**, 313 (1985).

[18] *Genie 2000 Spectroscopy Software Operations User'sManual*, *V3.1* (Canberra Industries. Inc., Meriden, CT, 2006).

[19] S. Y. F. Chu, L. P. Ekstrom, and R. B. Firestone, WWW table of radioactive isotopes, The Lund/LBNL nuclear data search. http://nucleardata.nuclear.lu.se/toi/index.asp/, 1999 (Accessed 24 April 2020).

[20] Live chart of nuclides: Nuclear structure and decay data, NDS, IAEA. https://www-nds.iaea.org/relnsd/vcharthtml/VChartHTML.html/, 2019 (Accessed 24 April 2020).

[21] WWW chart of the nuclides, Japanese nuclear data library. https://wwwndc.jaea.go.jp/CN14/index.html/, 2014 (Accessed 24 April 2020).

[22] Table of γ-rays, nuclear data center, korean atomic energy research institute (KAERI), http://atom.kaeri.re.kr/, 2015 (Accessed 24 April 2020).

[23] T. W. Burrows, Nuclear data sheets for $A = 48$, Nucl. Data Sheets **107**, 1747 (2006).

[24] S.-C. Wu, Nuclear data sheets for $A = 181$, Nucl. Data Sheets **106**, 367 (2005).

[25] Balraj Singh, Nuclear data sheets for $A = 182$, Nucl. Data Sheets **130**, 21 (2015).

[26] E. Achterberg, O. A. Capurro, and G. V. Marti, Nuclear data sheets for $A = 178$, Nucl. Data Sheets **110**, 1473 (2009).

[27] E. A. McCutchan, Nuclear data sheets for $A = 180$, Nucl. Data Sheets **126**, 151 (2015).

[28] J. F. Ziegler, M. D. Ziegler, and J. P. Biersack, SRIM-2013 code. http://srim.org. (Accessed 24 April 2018).

[29] *Guide to the Expression of Uncertainty of Measurement*, Ref. No. ISO/IEC GUIDE 98-3:2008(E) (International Organization for Standardization, Geneva, 2004).

[30] A. J. Koning, S. Hilaire, and M. C. Duijvestijn, TALYS -1.0, in *Proceedings of the International Conference on Nuclear Data for Science and Technology*, April 22 -27, 2007, Nice, France, edited by O. Bersillon, F. Gunsing, E. Bauge, R. Jacqmin, and S. Leray (EDP Sciences, Les Ulis, France, 2008), pp. 211–214.

[31] R. Capote, M. Herman, P. Obložinský, P. G. Young, S. Goriely, T. Belgya, A. V. Ignatyuk, A. J. Koning, S. Hilaire, V. A. Plujko, M. Avrigeanu, O. Bersillon, M. B. Chadwick, T. Fukahori, G. Zhigang, Y. Han, S. Kailas, J. Kopecky, V. M. Maslov, and G. Reffo *et al.* RIPL - Reference input parameter library for calculation of nuclear reactions and nuclear data evaluations, Nucl. Data Sheets **110**, 3107 (2009).

[32] J. Raynal, Notes on ECIS94, CEA Saclay Report No. CEA-N-2772, French Atomic Energy Commission, Paris, France, 1994.

[33] A. J. Koning and J. P. Delaroche, Local and global nucleon optical models from 1 keV to 200 MeV, Nucl. Phys. A **713**, 231 (2003).

[34] A. J. Koning and M. Duijvestijn, A global pre-equilibrium analysis from 7 to 200 MeV based on the optical model potential, Nucl. Phys. A **744**, 15 (2004).

[35] A. J. Koning, S. Hilaire, and M. Duijvestijn, TALYS: Comprehensive nuclear reaction modeling, in *International Conference on Nuclear Data for Science and Technology*, September 26 - October 1, 2004, Santa Fe, New Mexico, edited by R. C. Haight, M. B. Chadwick, T. Kawano, and P. Talou (AIP Conf. Proc. 769, Melville, NY, 2005), pp. 1154–1159.

[36] M. Herman, R. Capote, B. V. Carlson, P. Obložinský, M. Sin, A. Trkov, H. Wienke, and V. Zerkin, EMPIRE: Nuclear reaction model code system for data evaluation, Nucl. Data Sheets **108**, 2655 (2007).

[37] T. Belgya, O. Bersillon, R. Capote, T. Fukahori, G. Zhigang, S. Goriely, M. Herman, A. V. Ignatyuk, S. Kailas, A. Koning, P. Obložinský, V. Plujko, and P. Young, *Handbook for Calculations of Nuclear Reaction Data*, RIPL-2, IAEA-TECDOC-1506 (IAEA, Vienna, 2006).

[38] P. J. Daly, K. Ahlgren, K. J. Hofstetter, and R. Hochel, The level structure of ^{181}W from the decay of ^{181}Re, Nucl. Phys. A **161**, 177 (1971).

[39] F. Tárkányi, F. Ditrói, S. Takács, and A. Hermanne, New measurements of excitation functions of ^{186}W(p,x) nuclear reactions up to 65 MeV. Production of a ^{178}W / ^{178m}Ta generator, Nucl. Instrum. Methods Phys. Res. B **391**, 27 (2017).